Low-Cost Performance-Driven Modelling of Compact Microwave Components with Two-Layer Surrogates and Gradient Kriging

Slawomir Koziel[1,2] and Anna Pietrenko-Dabrowska[2]

[1] Engineering Optimization & Modeling Center, Reykjavik University, 101 Reykjavik, Iceland, koziel@ru.is,

[2] Faculty of Electronics, Telecommunications and Informatics, Gdansk University of Technology, 80-233 Gdansk, Poland, anna.dabrowska@pg.edu.pl

Keywords: Microwave design; compact microwave components; surrogate modeling; gradient kriging; domain confinement; simulation-driven design; design optimization.

Abstract

Utilization of electromagnetic (EM) simulation tools has become indispensable for reliable evaluation of microwave components. As the cost of an individual analysis may already be considerable, the computational overhead associated with EM-driven tasks that require massive simulations (e.g., optimization) may turn prohibitive. One of mitigation methods is the employment of equivalent network models. Yet, they are incapable of accounting for cross-coupling effects that occur in devices of complex geometries. Another option are fast replacement models (surrogates), especially the data-driven ones: readily available, generic and problem independent. Unfortunately, due to the curse of dimensionality, their applicability is limited to low-dimensional parameter spaces and narrow parameter ranges. From the utility perspective, however, the surrogate has to be valid over broad ranges of parameters and operating conditions. The recently reported performance-modeling techniques (especially nested-kriging) allow for rendering such surrogates even for complex devices. Key concept is to carry out the modeling process within a confined domain, being a subset of the parameter space that encompasses the designs of high-quality regarding the performance figures of choice. The goal of this work is to reduce the cost of reference design acquisition, which adds up to the total cost of constructing the surrogate. Toward this end, gradient-enhanced kriging is incorporated into the performance-driven modeling framework. The predictive power of the surrogates rendered using our approach by far exceeds that of the conventional methods and is comparable to the original nested kriging technique while requiring a significantly smaller number of reference designs (thus, the CPU cost). These features are demonstrated using a three-section transformer and a rat-race coupler.

1. Introduction

Design of contemporary miniaturized microwave components is heavily dependent on full-wave electromagnetic (EM) simulation analysis. This is mainly due incapability of analytical or equivalent network models to account for cross-coupling effects within densely arranged layouts of compact devices [1]-[3]. Among numerous examples of such structures, components implemented by folding conventional transmission lines [4], [5] as well as employing slow-wave structures [6], [7], or defected ground structures (DSGs) [8], [9] may be listed. The design process may become even more intricate when additional functionalities are required, e.g. multi- [10] or wide-band operation [11], but also harmonic attenuation [12], [13]. In consequence, topologies of compact microwave components are increasingly complex, and, more often than not, described by large numbers of designable parameters. As simultaneous adjustment of circuit parameters in highly-dimensional spaces is virtually impossible through experience-based parameter sweep, rigorous numerical optimization becomes imperative. This, in turn, entails massive EM simulations leading to substantial computational expenditures.

Perhaps the most straightforward approaches to accelerating EM-based numerical optimization are the algorithmic methods, where costly finite-differentiation-based sensitivity updates are replaced by sparse updates (e.g., Jacobian variability tracking [14], design relocation monitoring [15]), or restricted to the most important directions in the parameter space (e.g., corresponding to maximum variability of the system responses [16]). Another option is to utilize adjoint sensitivities, which is particularly advantageous for larger-scale problems [17]. From the computational efficiency point of view, another attractive alternative to EM-based numerical optimization are surrogate-assisted optimization methods, where the computational burden is shifted to a faster representation of the device under design, referred to as the surrogate model. In high-frequency engineering, the most popular group of

surrogates are data-driven models: flexible, readily available through Matlab toolboxes and easily adjustable to specific application requirements. Various approximation surrogates have been developed, including radial-basis functions [18], kriging interpolation [19], support-vector regression [20], or neural networks [21], [22]. Yet, their applicability is strongly limited to rather low-dimensional cases due to the curse of dimensionality, i.e., a rapid growth of the training set size with both the dimensionality of parameter space and the parameter ranges [23]. This issue is especially pronounced in high-frequency design, where typical responses of microwave components exhibit a high degree of nonlinearity [24]. Therefore, data-driven modeling of such structures is computationally feasible provided that the number of parameters is small and/or their ranges are sufficiently narrow.

Another group of models is physics-based surrogates. These are not as much affected by the curse of dimensionality as the approximation ones. Yet, they are also more problem specific, due to their dependence on underlying low-fidelity models, typically equivalent networks [25], or coarse-mesh EM simulations [26]. Embedding the knowledge about the device under design in the low fidelity model allows for addressing the curse of dimensionality, but, at the same time, significantly restricts the application area to the particular design case the surrogate was rendered for. Among the various techniques exploiting physics-based surrogates space mapping [27], adaptive response scaling [28], or feature-based optimization [29] may be enumerated.

In this work, we focus on an alternative approach to surrogate modeling, in which the construction of the surrogate is carried out from the standpoint of the performance figures relevant to a specific design context. This is referred to as performance-driven modeling [30]. The most prominent example is the nested kriging framework [31]. The performance-driven techniques [32]-[34] exploit the concept of a surrogate domain confinement, and involve a set of reference designs, pre-optimized with respect to the selected figures of interest. The

modeling process is limited to the region containing high-quality designs, spanned by the mentioned reference points. This allows for a dramatic reduction of the domain volume in comparison to conventional box-constrained domains, determined through the lower and upper bounds on the design variables. With the use of performance-driven frameworks, accurate surrogates are rendered at a fraction of cost required by conventional surrogates. Nevertheless, an unresolved issue of these methods is the initial computational overhead related to the reference design acquisition. Clearly, in some cases, these designs may be available from previous work on the same structure. In other cases, a designer may regard the initial effort of obtaining them justified by an intended multiple use of the model (e.g., for the purpose of the device re-design). Finally, domain confinement may prove the only approach capable of rendering reliable surrogate, in which case the reference design acquisition cost becomes a necessary sacrifice to construct the model at all.

The key concept of our method is to reduce the number of the reference points required to define the confined domain. This is achieved by employing the gradient-enhanced kriging technique (GEK) [35], being a variation of widely used kriging interpolation that allows for incorporating, as the training data, not only the system responses, but their gradients as well. In the original nested kriging technique, two kriging models are rendered: the first one sets the domain for the second, being the actual surrogate. Whereas in this work, the first-level model is a GEK-based one, set up with a reduced number of the reference designs. The proposed framework is demonstrated using two high-frequency devices: a rat-race coupler and a three-section impedance matching transformer. It is also favourably benchmarked against the basic nested kriging along with conventional kriging interpolation, showing excellent model accuracy even for small data set sizes where conventional techniques fail to render reliable surrogates. Incorporating the knowledge about the response sensitivity into the GEK-based first-level model, permitted to precisely delimit the confined

domain with the use of a smaller number of reference designs than in the original nested kriging framework (the number of the reference points is reduced over twofold for the coupler and as much as three times for the transformer). At the same time, the surrogate predictive power is maintained at a comparable level as for nested kriging.

2. Two-Layer Surrogate Modeling with Gradient-Enhanced-Kriging First-Level Model

This section introduces the proposed two-layer performance-driven modelling framework with the first-level surrogate being a gradient-enhanced kriging (GEK) model [35]. First, the performance-driven modelling approach within confined domain is briefly recalled. The following sections provide the formulation of the gradient kriging technique, delineate the overall nested-kriging framework exploiting GEK-based first-level model, and its employment for domain definition purposes.

2.1. Domain Confinement and Performance-Driven Modelling Concept

In performance-driven modelling [31], instead of conventionally setting up the surrogate from the parameter space perspective, the overall modelling process is carried on from the viewpoint of the design objectives. More specifically, it is conducted within a subset of the parameter space containing the designs that are optimum with respect to the figures of interest relevant for the structure under design. The performance figures may refer to operating conditions/requirements (e.g., operating frequency and power split ratio in the case of a coupler, or operating band for a filter or an impedance transformer) and/or the substrate parameters (e.g., relative permittivity). Constricting the surrogate domain as described above, brings considerable benefits from the point of view of the cost of training data acquisition. This is because the confined domain is considerably smaller than the conventional interval-type domain delimited by the lower and upper bounds on the design variables.

Let f_k, $k = 1, \ldots, N$, denote the performance figures. The surrogate model is to be valid within the region of the objective space determined by their ranges $f_{k.\min} \leq f_k^{(j)} \leq f_{k.\max}$, $k = 1, \ldots, N$. Whereas the vector of the geometry parameters of the device at hand is denoted as $\boldsymbol{x} = [x_1 \ldots x_n]^T$, and the lower and upper bounds on the parameters: $\boldsymbol{l} = [l_1 \ldots, l_n]^T$ and $\boldsymbol{u} = [u_1 \ldots, u_n]^T$, respectively, define the parameter space in the conventional sense.

Let also $U(\boldsymbol{x},\boldsymbol{f})$ be a scalar merit function encoding design specifications. The design $U_F(\boldsymbol{f})$, optimal for the objective vector $\boldsymbol{f} = [f_1 \ldots f_N]^T \in F$, is obtained by solving

$$U_F(\boldsymbol{f}) = \arg \min_{\boldsymbol{x}} U(\boldsymbol{x}, \boldsymbol{f}) \tag{1}$$

The set of the designs that are optimum with respect to all $\boldsymbol{f} \in F$ constitutes an N-dimensional manifold in the parameter space defined as

$$U_F(F) = \{U_F(\boldsymbol{f}) : \boldsymbol{f} \in F\} \tag{2}$$

Ideally, the surrogate should be constructed within $U_F(F)$. On the one hand, this allows us to integrate all the designs vital from the point of view of the performance figures relevant to a given design task. On the other hand, computational resources are not wasted on sampling the parts of the parameter space containing poor quality designs. A proper identification of the set $U_f(F)$ is crucial, yet, only its rough approximation is possible given limited data. Within performance-driven modelling framework, this approximation is performed based on the so-called reference designs $\boldsymbol{x}^{(j)} = [x_1^{(j)} \ldots x_n^{(j)}]^T$, $j = 1, \ldots, p$, that have been pre-optimized w.r.t. the selected objective vectors $\boldsymbol{f}^{(j)} = [f_1^{(j)} \ldots f_N^{(j)}]$ [31]. Uniform distribution of the vectors $\boldsymbol{f}^{(j)}$ within F is preferable.

If a given microwave structure has been previously designed (optimized) for various performance specifications, the set of the reference designs may already be available. Typically, however, the set of designs $\{\boldsymbol{x}^{(j)}\}_{j = 1, \ldots, p}$, has to be rendered specifically for a given modelling task, which requires performing p optimization runs the computational overhead of which is considerable.
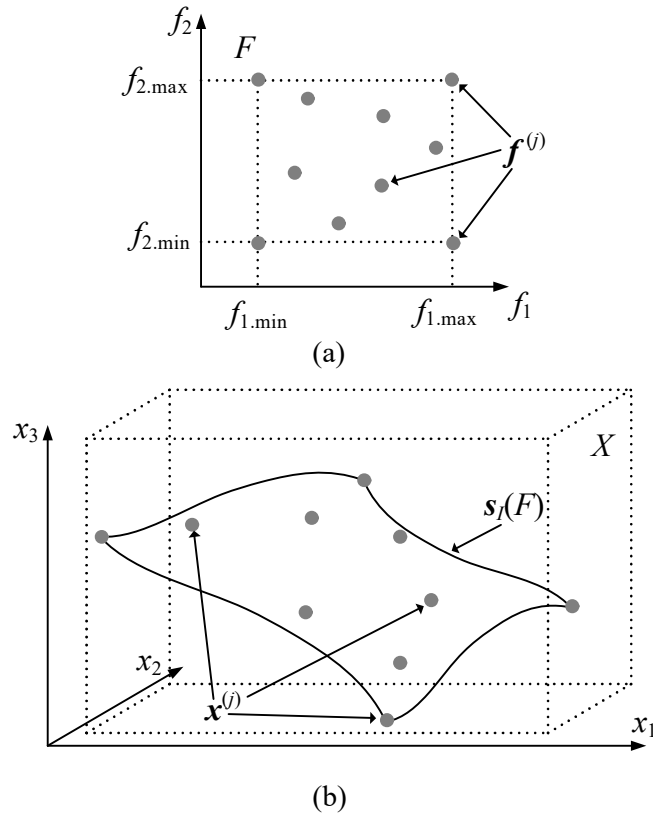
Fig. 1. Conceptual illustration of performance-driven modeling concept using nested kriging (for two- and three-dimensional objective and parameter space, respectively): (a) objective space F and the example allocation of the reference objective vectors $\boldsymbol{f}^{(j)}$ (gray circles), (b) parameter space X with the reference designs $\boldsymbol{x}^{(j)}$ shown, along with the first-level model image $\boldsymbol{s}_I(F)$.

Depending on the adopted performance-driven modelling technique, the actual ways of rendering the approximation of the manifold $U_F(F)$ by incorporating the reference points differ [30]-[34]. Our approach follows that of the nested-kriging framework [31], in which the optimum set $U_F(F)$ is approximated with the use of the first-level model $\boldsymbol{s}_I(\boldsymbol{f}) : F \rightarrow X$. The latter is a kriging surrogate set up based on the following training data set: $\{\boldsymbol{f}^{(j)}, \boldsymbol{x}^{(j)}\}$, $j = 1, \dots, p$ (cf. Fig. 1).

2.2. Kriging Interpolation with Gradients

Kriging [36] belongs to data-driven modelling techniques. It is widely-used in high-frequency electronics to interpolate EM-simulated noise-free data [37], [38]. Seeking computational savings, here, gradient-enhanced kriging (GEK) [35] is employed to decrease the number of the reference points necessary to approximate the manifold $U_F(F)$. GEK-based

surrogates, being a modification of ordinary kriging (OK), incorporate both the system output data and their gradients. In the following, gradient-enhanced kriging is briefly recapitulated for the convenience of the reader, for a more detailed exposition of the topic see, e.g, [23], [39].

A basic formulation of ordinary kriging (OK) assumes that the output $y(\boldsymbol{x})$ of the system at hand takes the following form [40]

$$y(\boldsymbol{x}) = \mu + Z(\boldsymbol{x}) \tag{3}$$

with $\boldsymbol{x}$ being the vector of designable variables. In (3), μ is the constant trend function and $Z(\boldsymbol{x})$ is a realization of a Gaussian random process (normally distributed with zero mean and variance σ^2, which accounts for localized variations from the mean μ). More generally, in (3), a low-order polynomial trend function μ may be used [36]

$$\mu = \boldsymbol{g}(\boldsymbol{x})^T \beta \tag{4}$$

For any given observation points $\boldsymbol{x}^{(i)}$ and $\boldsymbol{x}^{(j)}$, $i, j = 1, \ldots, p$, the correlations between $Z(\boldsymbol{x}^{(i)})$ and $Z(\boldsymbol{x}^{(j)})$ may be described by Gaussian correlation function [36]

$$R_{ij} = corr\left[Z(\boldsymbol{x}^{(i)}), Z(\boldsymbol{x}^{(j)}) \right] = \exp\left(-\sum_{k=1}^{n} \theta_k \mid x_k^{(i)} - x_k^{(j)} \mid^2 \right) \tag{5}$$

Another widely used formulation is a Matern 3/2 function [41]

$$R_{ij} = \left(1 + \sqrt{3\sum_{k=1}^{n} \theta_k \mid x_k^{(i)} - x_k^{(j)} \mid^2} \right) \exp\left(-\sqrt{3\sum_{k=1}^{n} \theta_k \mid x_k^{(i)} - x_k^{(j)} \mid^2} \right) \tag{6}$$

The system response at the observation point $\boldsymbol{x}$ is predicted as

$$s(\boldsymbol{x}) = \mu + \boldsymbol{r}(\boldsymbol{x})^T \boldsymbol{\Psi}^{-1}(\boldsymbol{y} - \boldsymbol{1}\mu) \tag{7}$$

In (7), $\boldsymbol{r}(\boldsymbol{x})$ stands for the vector of correlations between the p data samples $\boldsymbol{x}^{(j)}$ and $\boldsymbol{x}$, $\boldsymbol{\Psi}$ denotes a symmetric $p \times p$ matrix of correlations ψ_{ij} (cf. (5) and (6)); $\boldsymbol{1}$ is the vector containing ones, whereas $\boldsymbol{y}$ is the vector of the system outputs at $\boldsymbol{x}^{(j)}, j = 1, \ldots, p$. In order to

identify the model (7), optimization of the hyperparameter vector $\boldsymbol{\theta} = [\theta_1 \ \ldots \ \theta_n]^T$ is required. This is realized through maximum likelihood [36], i.e.,

$$-\frac{\left[p \ln\left(\sigma(\boldsymbol{\theta})^2\right) + \ln\left|\boldsymbol{\Psi}(\boldsymbol{\theta})\right| \right]}{2} \tag{8}$$

where the dependence of both σ^2 and $\boldsymbol{\Psi}$ on the hyperparameter vector $\boldsymbol{\theta}$ has been shown explicitly.

The GEK technique employs both the gradient data and response data to construct the surrogate, therefore, it may be regarded as a multi-data variation of ordinary kriging [35]. The GEK correlation matrix is created as

$$\dot{\boldsymbol{\Psi}} = \begin{bmatrix} \boldsymbol{\Psi} & \dfrac{\partial \boldsymbol{\Psi}}{\partial \boldsymbol{x}^{(i)}} \\ \dfrac{\partial \boldsymbol{\Psi}}{\partial \boldsymbol{x}^{(j)}} & \dfrac{\partial^2 \boldsymbol{\Psi}}{\partial \boldsymbol{x}^{(i)} \partial \boldsymbol{x}^{(j)}} \end{bmatrix} \tag{9}$$

Given the set of observations $\boldsymbol{x}^{(j)}$, $j = 1, \ldots, p$, and the observed data $\boldsymbol{y} = [y(\boldsymbol{x}^{(1)}) \ \ldots \ y(\boldsymbol{x}^{(p)}) \ \partial y(\boldsymbol{x}^{(1)})/\partial x_1 \ \ldots \ \partial y(\boldsymbol{x}^{(p)})/\partial x_1 \ \ldots \ \partial y(\boldsymbol{x}^{(1)})/\partial x_n \ \ldots \ \partial y(\boldsymbol{x}^{(p)})/\partial x_n]^T$, the GEK prediction is obtained as

$$s_{GEK}(\boldsymbol{x}) = \mu + \dot{\boldsymbol{r}}(\boldsymbol{x})^T \dot{\boldsymbol{\Psi}}^{-1}(\boldsymbol{y} - \boldsymbol{1}\mu) \tag{10}$$

with $\dot{\boldsymbol{r}}(\boldsymbol{x}) = \left[\boldsymbol{r}^T \ (\partial \boldsymbol{r} / \partial x_1)^T \ \ldots (\partial \boldsymbol{r} / \partial x_n)^T \right]$ being the correlation vector and the mean of the kriging regression expressed as

$$\mu = \left(\boldsymbol{1}^T \dot{\boldsymbol{\Psi}}^{-1} \boldsymbol{1} \right)^{-1} \boldsymbol{1}^T \dot{\boldsymbol{\Psi}}^{-1} \boldsymbol{y} \tag{11}$$

The mean μ is obtained by employing the generalized least squares. In GEK interpolation, the hyperparameters $\boldsymbol{\theta}$ are estimated in the same manner as in the case of OK, i.e., through maximum likelihood [36]. It should be noted that generalization of derivative-free (OK) and sensitivity-based (GEK) techniques for vector-valued outputs of microwave components may be performed directly.

2.3. Gradient-Enhanced-Nested-Kriging Framework

In this section, blending of the gradient-enhanced kriging into the nested-kriging framework is outlined. As opposed to the basic version of the nested-kriging modelling, here, the GEK-based first-level model is utilized. By incorporating gradient data, a significant decrease in the total number of reference points needed to set up the surrogate is possible, which is corroborated by the results presented in Section 3.

Following Section 2.1, let us briefly recollect that the first-level model $s_I(f)$, utilized in the basic nested kriging technique for domain confinement purposes, is constructed with the following training data set: $\{f^{(j)}, x^{(j)}\}$, $j = 1, \ldots, p$. Therein, $f^{(j)}$ are the objective vectors and $x^{(j)}$ denote the geometry parameter vectors of the microwave component under design optimized in the sense of (2). In most cases, the number of performance figures is not greater than three, therefore, $s_I(F)$ is a low-dimensional manifold in the parameter space X. As a consequence, the total number of the reference designs p may be efficiently reduced by incorporating the sensitivity data $J^x(f) = \partial x/\partial f = \partial U_F(f)/\partial f$ through the gradient-enhanced kriging technique delineated in Section 2.2. The Jacobian $J^x(f)$ consists of the partial derivatives J_{jk}^x of the (optimized) parameters of the component at hand with respect to the figures of interest f_k. Their assessment does not entail considerable computation expenses, as it is possible to estimate them based on the response sensitivities being a by-product of reference designs acquisition (cf. (2)).

Let $R(x)$ denote the EM-simulated response of the microwave device under design and $J_R(x) = \partial R/\partial x$ stand for Jacobian matrix at the design x. In addition, $d = [d_1 \ldots d_N]^T$ denotes a vector whose entries are perturbations of the figures of interests. The shifted reference designs $x^{(j,k)}$ for the vectors $[f_1^{(j)} \ldots f_k^{(j)} + d_k \ldots f_N^{(j)}]^T$ are obtained as

$$x^{(j.k)} = \arg \min_x U_L(x; f_1^{(j)}, ..., f_k^{(j)} + d_k, f_N^{(j)}) \tag{12}$$

In (12), U_L stands for the objective function (linear approximation of the response R)

$$R(x) = R(x^{(j)}) + J_R(x^{(j)}) \cdot (x - x^{(j)}) \tag{13}$$

Due to the fact that $J_R(x)$ is known in advance, solving of (9) does not entail any significant computational overhead. Once perturbed designs $x^{(j,k)}$ are found, the extraction of the actual values of the performance figures from $R(x^{(j,k)}$ has to be performed at the cost of a single EM simulation.

As the finite differences d_k are small, the following holds

$$x_l^{(j,k)} \approx x_l^{(j)} + \sum_{r=1}^{N} J_{lr}^x(x^{(j)})[f_r^{(j,k)} - f_r^{(j)}] \tag{14}$$

or in the matrix form

$$X = J^x F \tag{15}$$

where

$$X = \begin{bmatrix} x^{(j,1)} - x^{(j)} & \cdots & x^{(j,N)} - x^{(j)} \end{bmatrix} \tag{16}$$

and

$$F = \begin{bmatrix} f_1^{(j,1)} - f_1^{(j)} & \cdots & f_1^{(j,N)} - f_1^{(j,N)} \\ \vdots & \ddots & \vdots \\ f_N^{(j,1)} - f_N^{(j)} & \cdots & f_N^{(j,N)} - f_N^{(j,N)} \end{bmatrix} \tag{17}$$

The above can be solved analytically for J^x provided the matrix F is invertible

$$J^x = XF^{-1} \tag{18}$$

As off-diagonal entries of the matrix F are typically small, therefore, despite $[f_1^{(j,k)} \dots f_N^{(j,k)}]^T \neq [f_1^{(j)} \dots f_k^{(j)} + d_k \dots f_N^{(j)}]^T$, F is a non-singular matrix. In the case, when $F = \text{diag}(d_1,\dots,d_N)$ (i.e., it is diagonal and we have $[f_1^{(j,k)} \dots f_N^{(j,k)}]^T = [f_1^{(j)} \dots f_k^{(j)} + d_k \dots f_N^{(j)}]^T$), the following holds

$$x_l^{(j,k)} \approx x_l^{(j)} + J_{lk}^x(x^{(j)})d_k \tag{19}$$

and consequently (18) coincides with the following

$$J_{lk}^{x}(\boldsymbol{x}^{(j)}) \approx \left[x_{l}^{(j.k)} - x_{l}^{(j)} \right] / d_{k} \tag{20}$$

The training data set for GEK-based first-level model $\boldsymbol{s}_{I.GEK}(\boldsymbol{f})$ is $\{\boldsymbol{f}^{(j)}, \boldsymbol{x}^{(j)}, \boldsymbol{J}^{x}(\boldsymbol{f}^{(j)})\}$, $j = 1$, …, p. By incorporating the sensitivity data into $\boldsymbol{s}_{I.GEK}(\boldsymbol{f})$, a number of data samples required to render the surrogate is greatly reduced in comparison to the original (derivative-free) version of the technique.

2.4. Confined Domain and Construction of Second-Level Model

The model $\boldsymbol{s}_{I.GEK}(\boldsymbol{f})$ is a mere approximation of the manifold $U_{F}(F)$, therefore an extension is necessary in order to ensure that most of the designs $U_{F}(\boldsymbol{f})$ are encompassed within the confined domain X_{S}. Toward this end, the vectors normal to $\boldsymbol{s}_{I.GEK}(F)$ are employed. Let $\{\boldsymbol{v}_{n}^{(k)}(\boldsymbol{f})\}$, $k = 1$, …, $n - N$, denote an orthonormal basis of vectors normal to $\boldsymbol{s}_{I.GEK}(F)$ at the objective vector $\boldsymbol{f}$. Based upon this, the extension coefficients are defined as

$$\boldsymbol{\alpha}(\boldsymbol{f}) = [\alpha_{1}(\boldsymbol{f}) \dots \alpha_{n-N}(\boldsymbol{f})]^{T} = 0.5T \left[|\boldsymbol{x}_{d}\boldsymbol{v}_{n}^{(1)}(\boldsymbol{f})| \ \dots \ |\boldsymbol{x}_{d}\boldsymbol{v}_{n}^{(n-N)}(\boldsymbol{f})| \right]^{T} \tag{21}$$

In (21), $\boldsymbol{x}_{d} = \boldsymbol{x}_{max} - \boldsymbol{x}_{min}$ represents parameter variations within $\boldsymbol{s}_{I.GEK}(F)$, whereas $\boldsymbol{x}_{max} = \max\{\boldsymbol{x}^{(k)}, k = 1, …, p\}$ and $\boldsymbol{x}_{min} = \min\{\boldsymbol{x}^{(k)}, k = 1, …, p\}$. In addition, T stands for a user-defined parameter defining the domain lateral dimensions (its typical values vary from 0.025 to 0.1).
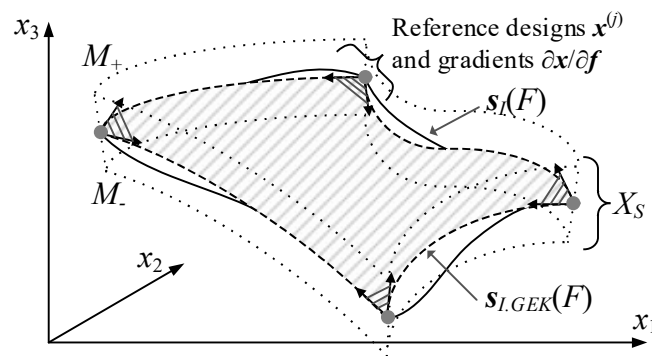

Fig. 2. Graphical explanation of the image $\boldsymbol{s}_{I.GEK}(F)$ of the gradient-enhanced kriging first-level model; the surrogate model domain X_{S} is delimited by the manifolds M_{-} and M_{+} and constitutes the orthogonal extension of $\boldsymbol{s}_{I.GEK}(F)$. In the example shown, the GEK-based surrogate first is rendered with the use of the corner reference designs $\boldsymbol{x}^{(j)}$ only, along with their corresponding sensitivities $\partial \boldsymbol{x} / \partial \boldsymbol{f} = \partial U_{F}(\boldsymbol{f}^{(j)}) / \partial \boldsymbol{f}$ indicated by arrows and gray shading.

The domain X_S is delimited by the manifolds M_+ and M_-

$$M_\pm = \left\{ x \in X : x = s_{I.GEK}(f) \pm \sum_{k=1}^{n-N} \alpha_k(f) v_n^{(k)}(f) \right\} \tag{22}$$

Hence, the definition of the constricted domain is as follows (see also Fig. 2)

$$X_S = \left\{ \begin{array}{l} x = s_{I.GEK}(f) + \sum_{k=1}^{n-N} \lambda_k \alpha_k(f) v_n^{(k)}(f) : f \in F, \\ -1 \le \lambda_k \le 1, k = 1, ..., n - N \end{array} \right\} \tag{23}$$

The second-level model is a derivative-free kriging surrogate set up in the very domain defined by (23) (cf. [34]) with $\{ x_B^{(k)}, R(x_B^{(k)}) \}_{k=1, ..., N_B}$, being the training data set. The samples $x_B^{(k)}$ are uniformly distributed within X_S, and R stands for the response of the microwave component at hand. For details on design of experiments as well as model optimization procedures see [31], [34].

The main benefit of surrogate domain confinement as described above is relatively small data set sizes required for setting up reliable surrogates (typically, a few hundred [33], [34]). At the same time, the ranges of neither the system parameters nor operating conditions have to be restricted. This sort of performance is not achievable for traditional (unconstrained) modeling methods, particularly in higher-dimensional spaces. It is quite common nowadays that the number of parameters exceeds ten or even twenty, for example, in the case of miniaturized components that involve compact microstrip resonant cells (CMRCs) [42], [43]. For circuits of this complexity, rendering accurate surrogates in conventional domains is impossible even with large number of data samples.

On the other hand, the cost of obtaining the reference designs may become the major contributor to the overall cost of setting up the model for performance-driven methods, by far exceeding the cost of training data acquisition within the constrained domain. Identifying the first-level model by means of GEK permits a significant reduction of these expenses, by fifty percent or more, as demonstrated in Section 3.

3. Verification Case Studies

This section discusses verification of the proposed modeling methodology. The verification cases include a rat-race coupler and a miniaturized impedance matching transformer. Comprehensive numerical studies have been conducted to demonstrate superiority of the GEK-based surrogates over the conventional kriging surrogates, as well as the basic nested kriging surrogates in terms of predictive power and potential computational savings.

3.1. Rat-race Coupler

The first verification structure is a microstrip rat-race coupler (RRC) [31] shown in Fig. 3(a). The device is implemented on RF-35 substrate ($\varepsilon_r = 3.5$, $h = 0.762$ mm, tan $\delta = 0.0018$), and its geometry is described by six parameters $\boldsymbol{x} = [l_1 \ l_2 \ l_3 \ d \ w \ w_1]^T$; with the following dimensions being fixed: $d_1 = d + |w - w_1|$, $d = 1.0$, $w_0 = 1.7$, and $l_0 = 15$ fixed (all in mm). The computational model of the RRC is implemented in CST Microwave Studio and evaluated using its frequency-domain EM solver (~90,000 mesh cells, simulation time ~6 minutes on Intel Xeon 2.1 GHz machine with 64 GB RAM).

The goal is to construct surrogates valid over the following ranges of the operating conditions: operating frequency f_0 varying from 1 GHz to 2 GHz, and the power split ratio $K = |S_{21}| - |S_{31}|$ ranging from –6 dB to 0 dB. The optimized design is to satisfy the following performance requirements: (i) obtaining the required power split K at f_0, and (ii) minimizing matching $|S_{11}|$ and isolation $|S_{41}|$ at f_0. The lower and upper bounds on the design variables are $\boldsymbol{l} = [2.0 \ 7.0 \ 12.5 \ 0.2 \ 0.7 \ 0.2]^T$, and $\boldsymbol{u} = [4.5 \ 12.5 \ 22.0 \ 0.65 \ 1.5 \ 0.9]^T$. The allocation of the reference designs utilized by both the basic nested kriging framework and the proposed gradient-enhanced nested kriging technique are provided in Figure 3(b) and Table 1. Whereas Fig. 4 shows a visual comparison of the first-level surrogates rendered in the original and GEK-based nested kriging for the selected geometry parameters. It should be noted that both

models are in a good agreement, despite a significant difference in the number of the reference designs they are set up with: as much as twelve for the former, and merely four for the latter. This has been achieved by incorporating the sensitivity data into the modelling process.

Table 1. Reference Design Allocation for the Original and the Proposed Gradient-Enhanced Nested Kriging Modeling Techniques for the Rat-Race Coupler of Fig. 3(a)

Reference Designs			
Original Nested Kriging [31]		Gradient-Based Nested Kriging[This Work]	
Design Pairs $\{f_0,K\}$	Number of Reference Designs [Overall Optimization Time *]	Design Pairs $\{f_0,K\}$ (objective space corners)	Number of Reference Designs [Overall Optimization Time *]
$\{1.0,0.0\}$, $\{1.0,-2.0\}$, $\{1.0,-6.0\}$, $\{1.2,-4.0\}$, $\{1.3,0.0\}$, $\{1.5,-5.0\}$, $\{1.5,-2.0\}$, $\{1.7,-6.0\}$, $\{1.7,0.0\}$, $\{1.8,-3.0\}$, $\{2.0,0.0\}$, $\{2.0,-6.0\}$	**12** **4380 min***	$\{1.0,0.0\}$, $\{1.0,-6.0\}$, $\{2.0,0.0\}$, $\{2.0,-6.0\}$,	**4** **1440 min***

*The total simulation time required for the reference design set acquisition; the duration of the single simulation equals 6 min.

Table 2. Modeling Results and Benchmarking for Rat-Race Coupler of Fig. 3(a))

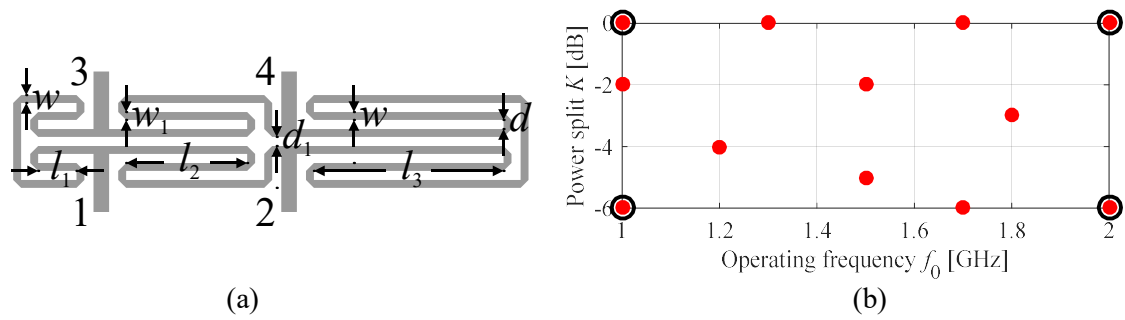| Number of Training Samples	Relative RMS Error			
	Conventional Kriging Model	Conventional RBF	Conventional Nested Kriging Model [31]	GEK-based Nested Kriging Model [this work]
50	25.7 %	28.3 %	6.9 %	5.8 %
100	17.9 %	19.1 %	5.7 %	3.9 %
200	13.5 %	13.9 %	3.8 %	3.4 %
400	9.9 %	10.3 %	3.5 %	2.9 %
800	8.0 %	8.9 %	3.1 %	2.3 %

Fig. 3. Microstrip rat-race coupler (RRC): (a) geometry [31], (b) allocation of the reference designs: conventional nested-kriging technique (solid circles) (12 reference points) versus proposed gradient-enhanced nested kriging technique (o) (only 4 reference points in the objective space corners).
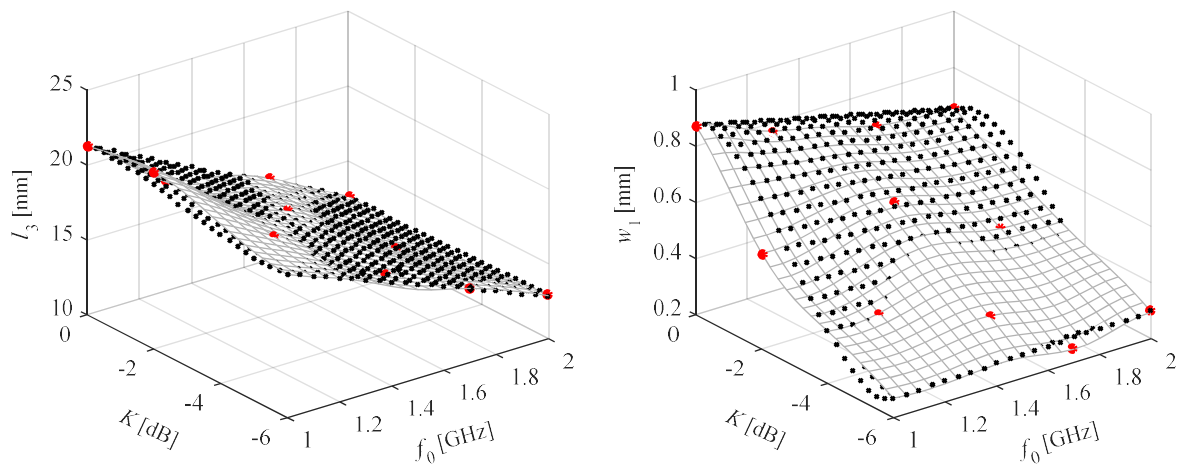

Fig. 4. Graphical illustration of the first-level models $s_I(\mathbf{f}) : F \rightarrow X$ for the selected design variables (l_3 and w_1) of the rat-race coupler plotted as functions of the performance figures of interest: the power split K and the operating frequency f_0: nested kriging (mesh surface) and GEK-based (black circles); red circles indicate the reference designs utilized by the original nested kriging technique (GEK-based first level model utilizes merely four designs allocated in the corners of the objective space F).

The proposed gradient-enhanced nested kriging surrogate model has been constructed for various numbers of the training data samples: 50, 100, 200, 400, and 800. Here, we employ the root mean square (RMS) error (averaged over the test set consisting of 100 independent samples) in order to compare the models. The proposed technique has been benchmarked against: (i) basic nested kriging utilizing the first-level model set up without incorporating the sensitivity data (for the number and allocation of the reference design see Fig. 4 and Table 1), (ii) conventional kriging model set up in box-constrained domain and, (iii) radial basis function models.
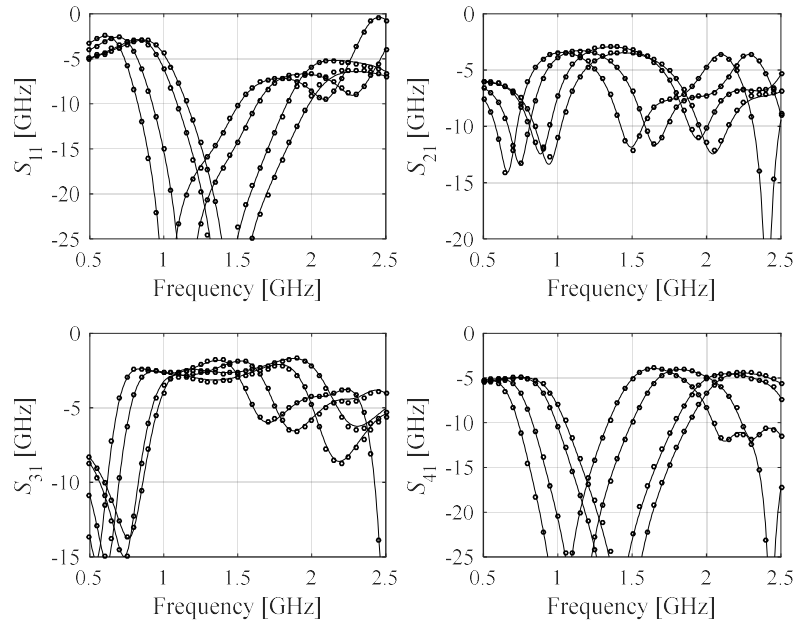
Fig. 5. Reflection characteristics of rat-race coupler of Fig. 3(a) at the selected test designs: EM simulation model (—), and the proposed GEK-based surrogate (o) (constructed using $N = 400$ training samples).

The thickness parameter (i.e., parameter T that defines the lateral dimensions of the constrained domain, cf. (21)) has been set to 0.05. Table 2 and Fig. 5 provide the numerical results. The predictive power of derivative-free and GEK-based nested kriging surrogates are significantly better than that of the conventional kriging and RBF models. Nevertheless, here, we intend to demonstrate that reducing the number of the reference designs to merely one third of the original set (twelve versus four for the nested and GEK-based kriging, respectively) does not have detrimental effect on the modeling accuracy. As a matter of fact, for this verification case, a certain accuracy improvement can be observed, which is the effect of the GEK-based first-level model surfaces being more regular than those of the original nested kriging.

As far as the computational cost of the reference design set acquisition is concerned, in the proposed framework, it is reduced by the factor of three in comparison to the original nested kriging procedure: from 730 simulations to 240 simulations (i.e., the simulation time

has been decreased from 4380 to 1440 minutes; see also Table 1). The GEK-based surrogate models can also be favourably compared to the benchmark techniques in terms of the number of simulations required to achieve comparable modeling accuracy. Within the conventional frameworks (RBF and kriging surrogates set up in conventional domains delimited by the lower and upper bounds on the designable parameters), the best accuracy of around 8 % has been obtained for the surrogates constructed using 800 data samples and their acquisition time has been equal to 4800 minutes. Whereas in the proposed technique, the comparable accuracy of 5 % has been achieved for merely 50 samples acquired within 300 minutes (i.e., the duration has been sixteen times shorter).

3.2. Three-Section Impedance Matching Transformer

The second verification case is the 50-to-100 Ohm impedance matching transformer (see Fig. 6(b)), in which conventional transmission lines are replaced by compact microstrip resonant cells (CMRCs) shown in Fig. 6(a). This allows for a reduction of the overall physical length of the device. The structure is described by the following designable variables $x = [l_{1.1}\ l_{1.2}\ w_{1.1}\ w_{1.2}\ w_{1.0}\ l_{2.1}\ l_{2.2}\ w_{2.1}\ w_{2.2}\ w_{2.0}\ l_{3.1}\ l_{3.2}\ w_{3.1}\ w_{3.2}\ w_{3.0}]^T$, and implemented on RF-35 substrate [31]. The design space is delimited by the lower and upper bounds on geometry parameters: $l = [2.0\ 0.15\ 0.65\ 0.35\ 0.30\ 2.70\ 0.15\ 0.44\ 0.15\ 0.30\ 3.2\ 0.15\ 0.30\ 0.15\ 0.30]^T$, and $u = [3.4\ 0.50\ 0.80\ 0.55\ 1.90\ 4.00\ 0.50\ 0.67\ 0.50\ 1.55\ 4.5\ 0.26\ 0.46\ 0.27\ 1.75]^T$, respectively. The computational model of the three-section transformer is implemented in CST Microwave Studio and evaluated using the time-domain solver (~320,000 mesh cells, simulation time ~2 minutes on Intel Xeon 2.1 GHz machine with 64 GB RAM).

In this verification case, the objective space is delimited by the following ranges of operating bands $[f_1\ f_2]$ (defined by $|S_{11}| \leq -20$ dB): with 1.5 GHz $\leq f_1 \leq$ 3.5 GHz, and 4.5 GHz $\leq f_2 \leq$ 6.5 GHz. The optimum design is to minimize of the maximum reflection $|S_{11}|$ within $[f_1\ f_2]$

(i.e., it is to be optimized in a minimax sense). The reference designs allocation for derivative-free and non-sensitivity-based nested kriging techniques are shown in Fig. 6(b) and Table 3. A visual comparison of the first-level surrogates rendered by both frameworks for the selected geometry parameters are shown in Fig. 7. As in the previous case, the two surrogates coincide with each other well (here, the following numbers of the reference point have been used: nine versus four, for the original and GEK-based technique, respectively).

Table 3. Reference Design Allocation for the Conventional and the Proposed Gradient-Enhanced Nested Kriging Modeling Techniques for the Three-Section Impedance Transformer of Fig. 6(b)

Reference Designs			
Original Nested Kriging [31]		Gradient-Based Nested Kriging[This Work]	
Design Pairs $\{f_1, f_2\}$	Number of Reference Designs [Overall Optimization Time *]	Design Pairs $\{f_1, f_2\}$ (objective space corners)	Number of Reference Designs [Overall Optimization Time *]
{1.5,4.5}, {1.5,5.5}, {1.5,6.5}, {2.5,4.5}, {2.5,5.5}, {2.5,6.5}, {3.5,4.5}, {3.5,5.5}, {3.5,6.5}	**9** **2890 min***	{1.5,4.5}, {1.5,6.5}, {3.5,4.5}, {3.5,6.5}	**4** **1270 min***

*The total simulation time required for the reference design set acquisition; the duration of the single simulation equals 6 min.

Table 4. Modeling Results and Benchmarking for Three-Section Transformer (Fig. 6(b))

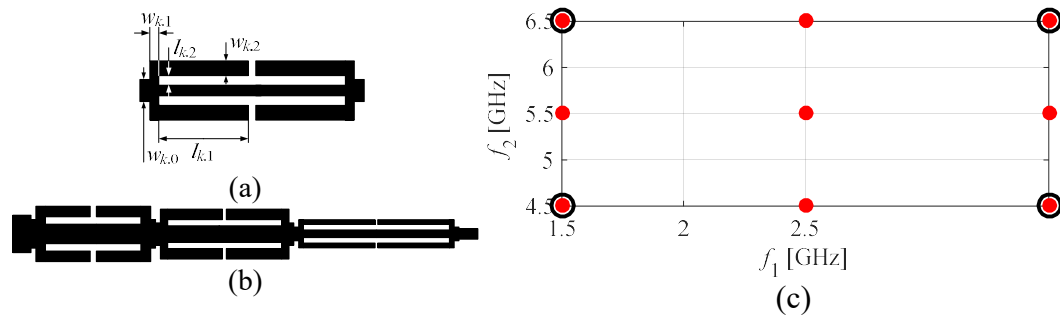| Number of Training Samples	Relative RMS Error			
	Conventional Kriging Model	Conventional RBF	Conventional Nested Kriging Model [31]	GEK-based Nested Kriging Model [this work]
50	49.1 %	56.2 %	17.3 %	14.6 %
100	31.1 %	33.0 %	13.9 %	9.3 %
200	25.9 %	27.5 %	10.3 %	7.2 %
400	20.4 %	23.1 %	7.4 %	7.1 %
800	15.7 %	16.8 %	6.1 %	5.1 %

Fig. 6. CMRC-based miniaturized three-section impedance transformer: (a) compact cell (CMRC), (b) transformer geometry [31], (c) allocation of the reference designs for the conventional nested-kriging technique (solid circles) (9 reference points) versus the proposed gradient-enhanced nested kriging technique (o) (only 4 reference points in the objective space corners).
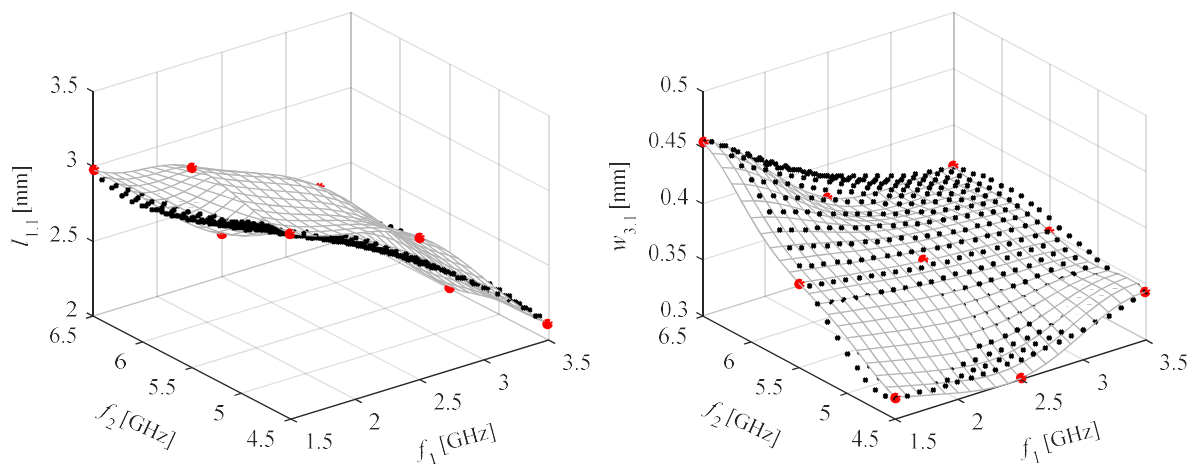

Fig. 7. Graphical illustration of the first-level models $s_I(f) : F \rightarrow X$ for the selected design variables ($l_{1.1}$ and $w_{3.1}$) of the transformer plotted as functions of the performance figures of interest, the left- and the right-hand-side ends of the operating bandwidth f_1 and f_2, respectively: nested kriging (mesh surface) and GEK-based (black circles); red circles indicate reference designs utilized by the original nested kriging technique (GEK-based first level model utilizes merely four designs allocated in the corners of the objective space F).
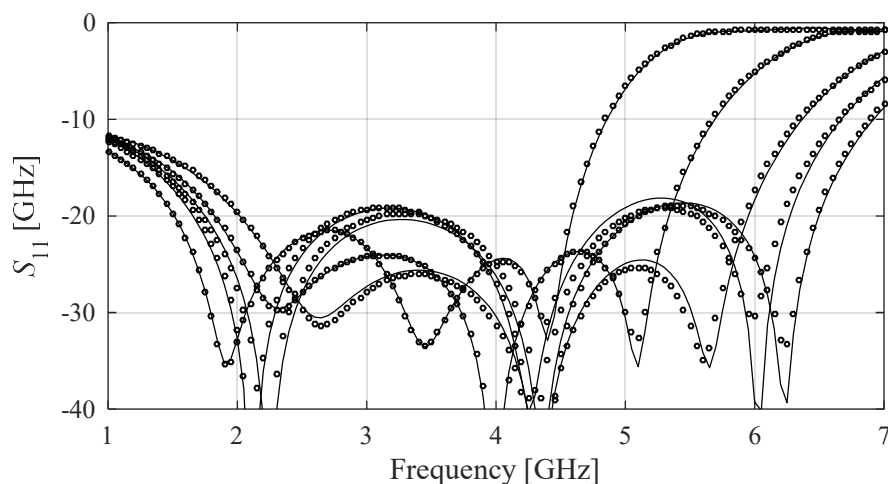

Fig. 8. Reflection characteristics of three-section transformer of Fig. 6(b) at the selected test designs: EM simulation model (—), and the proposed GEK-based surrogate (o) (constructed using $N = 400$ training samples).

Here, the proposed GEK-based kriging surrogate model has also been set up using the training data sets consisting of various number of samples: 50, 100, 200, 400, and 800. The modelling results and benchmarking are provided in Table 4 and Fig. 8. In the case of the transformer, the thickness parameter T defining the lateral dimensions of the surrogate domain, (see (21)) has also been set to 0.05. As in the previous verification case, the model accuracy of the original and GEK-based nested kriging surrogates are superior to those obtained within conventional frameworks (kriging interpolation and RBF surrogates). Despite the reduced number of the reference designs employed in setting up the first-level model, the predictive power of the gradient-enhanced surrogates is slightly better than that of the basic version of the technique.

Here, the computational cost of the reference designs acquisition is over twice lower than in the basic nested kriging technique: 1445 simulations versus 635 simulations (i.e., the simulation time has been reduced from 2890 to 1270 minutes; see also Table 3). Similarly as in the previous case study, the number of simulations necessary to ensure comparable model predictive power as the benchmark techniques is significantly lower. The best accuracy of the conventional surrogates is around 16 % and it has been obtained for the surrogates set up with 800 data samples (acquisition time of 1600 minutes). In our methodology, similar accuracy has been ensured for 50 samples acquired within 100 minutes (i.e., the duration has been sixteen times shorter). This corroborates computational efficiency and reliability of the GEK-based nested modeling framework.

5. Conclusion

In this work, a novel approach to reliable modelling of miniaturized microwave components has been proposed. The two fundamental ingredients of the presented technique are the recently reported nested kriging framework and gradient-enhanced kriging (GEK). The latter is employed to render the first-level surrogate, one of the domain-defining

components of the nested kriging. An essential part of blending GEK with nested kriging is a procedure for low-cost estimation of the geometry parameter sensitivities with respect to the figures interest relevant to the circuit at hand. These gradients are then incorporated into the first-level model in the form of the training data for the GEK-based surrogate. The principal advantage of the proposed methodology is a considerable reduction of the number of reference designs by at least fifty percent as compared to the traditional setup. This has a paramount importance for the reduction of the overall cost of the modelling process because each reference design requires pre-optimization. For the sake of validation, two compact microwave components have been considered, a rat-race coupler and an impedance matching transformer, both modelled over broad ranges of operating conditions. Comprehensive numerical comparisons indicate that reduction of the reference sets (from twelve to four points for the transformer and from nine to four points for the coupler) did not have any detrimental effects on the model predictive power across the various training data sets (from 50 to 800 samples) considered in the work. As a matter of fact, a certain accuracy improvement has been observed, which can be attributed to a more regular geometry of the GEK-based domain. It should be emphasized that reducing the number of required reference designs addresses one of the important practical issues of performance-driven modelling methods. Therefore, it can be viewed as a step toward a further improvement of their computational efficiency.

References

[1] Ting H, Hsu S, Wu T. A novel and compact eight-port forward-wave directional coupler with arbitrary coupling level design using four-mode control technology. IEEE Trans Microwave Theory Techn. 2017;65:467–475. https://doi.org/10.1109/TMTT.2016.2623709

[2] Koziel S, Kurgan P. Inverse modeling for fast design optimization of small-size rat-race couplers incorporating compact cells. Int J RF Microw Comput Aided Eng. 2018;28:e21240. https://doi.org/10.1002/mmce.21240

[3] Kurgan P, Koziel S. Selection of circuit geometry for miniaturized microwave components based on concurrent optimization of performance and layout area. AEU – Int J Electr Comm. 2019;108:287–294. https://doi.org/10.1016/j.aeue.2019.06.009

[4] Letavin D. Miniature microstrip branch line coupler with folded artificial transmission lines. AEU – Int J Electr Comm. 2019;99:8–13. https://doi.org/10.1016/j.aeue.2018.11.016

[5] Ameen M, Kumar Chaudhary R. A compact circularly polarized antenna using CRLH inspired transmission line and coupled ring resonator. AEU – Int J Electr Comm. 2020;121:153238. https://doi.org/10.1016/j.aeue.2020.153238

[6] Panigrahi R, Joy Thomas M, Vinoy KJ. A new fabrication method for serpentine-folded waveguide slow wave structure at W-Band. IEEE Trans Electron Devices. 2020;67:1198–1204. https://doi.org/10.1109/TED.2019.2963315

[7] Bertrand M, El Dirani H, Pistono E, Kaddour D, Puyal V, Ferrari P. A 3-dB coupler in slow wave substrate integrated waveguide technology. IEEE Microwave Wireless Comp Lett. 2019;29:270–272. https://doi.org/10.1109/LMWC.2019.2900239

[8] Fritz-Andrade E, Perez-Miguel A, Gomez-Villanueva R, Jardon-Aguilar H. Characteristic mode analysis applied to reduce the mutual coupling of a four-element

patch MIMO antenna using a defected ground structure. IET Microwaves Ant Propag. 2020;14:215–226. https://doi.org/10.1049/iet-map.2019.0570

[9] Kshore N, Upadhyay G, Shanker Tripathi V, Prakash A. Dual band rectangular patch antenna array with defected ground structure for ITS application. AEU – Int J Electr Comm. 2018;96:228–237. https://doi.org/10.1016/j.aeue.2018.09.039

[10] Gomez-Garcia R, Rosario-De Jesus J, Psychogiou D. Multi-band bandpass and bandstop RF filtering couplers with dynamically-controlled bands. IEEE Access. 2018;6:32321–32327. https://doi.org/10.1109/ACCESS.2018.2844868

[11] Wang X, Ma Z, Xie T, Ohira M, Chen C, Lu G. Synthesis theory of ultra-wideband bandpass transformer and its Wilkinson power divider application with perfect in-band reflection/isolation. IEEE Trans Microwave Theory Techn. 2019;67:3377–3390. https://doi.org/10.1109/TMTT.2019.2918539

[12] Li Y, Chen J, Lu Q, Qin W, Li W, Bao Z. A new and simple design approach for harmonic suppression in bandpass filter. IEEE Microw Wireless Comp Lett. 2017;27:126–128. https://doi.org/10.1109/LMWC.2016.2646922

[13] Rekha TK, Abdulla P, Jasmine PM, Anu AR. Compact microstrip lowpass filter with high harmonics suppression using defected structures. AEU – Int J Electr Comm. 2020;115:153032. https://doi.org/10.1016/j.aeue.2019.153032

[14] Pietrenko-Dabrowska A, Koziel S. Computationally-efficient design optimization of antennas by accelerated gradient search with sensitivity and design change monitoring. IET Microwaves Ant Propag. 2020;14:165–170. https://doi.org/10.1049/iet-map.2019.0358

[15] Koziel S, Pietrenko-Dabrowska A. Reduced-cost electromagnetic-driven optimization of antenna structures by means of trust-region gradient-search with sparse Jacobian

updates. IET Microwaves Ant Propag. 2019;13:1646–1652. https://doi.org/10.1049/iet-map.2018.5879

[16] Tomasson JA, Koziel S, Pietrenko-Dabrowska A. Expedited design closure of antenna input characteristics by trust region gradient search and principal component analysis. IEEE Access. 2020;8:8502–8511. https://doi.org/10.1109/ACCESS.2020.2964096

[17] Koziel S, Ogurtsov S, Cheng QS, Bandler JW. Rapid electromagnetic-based microwave design optimization exploiting shape-preserving response prediction and adjoint sensitivities. IET Microwaves Ant Propag. 2014;8:775–781. https://doi.org/10.1049/iet-map.2013.0636

[18] Chávez-Hurtado JL, Rayas-Sánchez JE. Polynomial-based surrogate modeling of RF and microwave circuits in frequency domain exploiting the multinomial theorem. IEEE Trans Microwave Theory Techn, 2016;64:4371–4381. https://doi.org/10.1109/TMTT.2016.2623902

[19] Passos F, González-Echevarría R, Roca E, Castro-Lopez R, Fernandez FV. A two-step surrogate modeling strategy for single-objective and multi-objective optimization of radiofrequency circuits. Soft Comput. 2019;23:4911–4925. https://doi.org/10.1007/s00500-018-3150-9

[20] Cai J, King J, Yu C, Liu J, Sun L. Support vector regression-based behavioral modeling technique for RF power transistors. IEEE Microw Wireless Comp Lett. 2018;28:428–430. https://doi.org/10.1109/LMWC.2018.2819427

[21] Jin J, Zhang C, Feng F, Na W, Ma J, Zhang Q. Deep neural network technique for high-dimensional microwave modeling and applications to parameter extraction of microwave filters. IEEE Trans Microwave Theory Techn. 2019;67:4140–4155. https://doi.org/

10.1109/TMTT.2019.2932738

[22] Ustun D, Toktas A, Akdagli A. Deep neural network–based soft computing the resonant frequency of E–shaped patch antennas. AEU – Int J Electr Comm. 2019;102:54–61. https://doi.org/10.1016/j.aeue.2019.02.011

[23] Forrester AIJ, Keane AJ. Recent advances in surrogate-based optimization. Progr Aerosp Sci. 2009;45:50–79. https://doi.org/10.1016/j.paerosci.2008.11.001

[24] Goudos S. Design of microwave broadband absorbers using a self-adaptive differential evolution algorithm. Int J RF Microw Comput Aided Eng. 2009;19:364–372. https://doi.org/10.1002/mmce.20357

[25] Gorissen D, Zhang L, Zhang QJ, Dhaene T. Evolutionary neuro-space mapping technique for modeling of nonlinear microwave devices. IEEE Trans Microwave Theory Techn. 2011;59:213–229. https://doi.org/10.1109/TMTT.2010.2090169

[26] Feng F, Zhang J, Zhang W, Zhao Z, Jin J, Zhang QJ. Coarse- and fine-mesh space mapping for em optimization incorporating mesh deformation. IEEE Microw Wireless Comp Lett. 2019;29:510–512. https://doi.org/10.1109/LMWC.2019.2927113

[27] Rayas-Sanchez JE. Power in simplicity with ASM: tracing the aggressive space mapping algorithm over two decades of development and engineering applications. IEEE Microw Magazine. 2016;17:64–76. https://doi.org/10.1109/MMM.2015.2514188

[28] Koziel S, Bandler JW, Madsen K. Space mapping with adaptive response correction for microwave design optimization. IEEE Trans Microwave Theory Techn. 2009;57:478–486. https://doi.org/10.1109/TMTT.2008.2011243

[29] Koziel S, Pietrenko-Dabrowska A. Design-oriented computationally-efficient feature-based surrogate modelling of multi-band antennas with nested kriging. AEU – Int J Electr Comm. 2020;120:153202. https://doi.org/10.1016/j.aeue.2020.153202

[30] Koziel S, Pietrenko-Dabrowska A. performance-driven surrogate modeling of high-frequency structures. New York: Springer; 2020.

[31] Koziel S, Pietrenko-Dabrowska A. Reduced-cost surrogate modeling of compact microwave components by two-level kriging interpolation. Eng Optim. 2019;52:960–972. https://doi.org/10.1080/0305215X.2019.1630399

[32] Koziel S, Low-cost data-driven surrogate modeling of antenna structures by constrained sampling. IEEE Ant Wireless Propag Lett. 2017;16:461–464. https://doi.org/10.1109/LAWP.2016.2583474

[33] Koziel S, Sigurðsson AT. Triangulation-based constrained surrogate modeling of antennas. IEEE Trans Ant Propag. 2018;66:4170–4179. https://doi.org/10.1109/TAP.2018.2839759

[34] Koziel S, Pietrenko-Dabrowska A. Performance-based nested surrogate modeling of antenna input characteristics. IEEE Trans Ant Propag. 2019;67:2904–2912. https://doi.org/10.1109/TAP.2019.2896761

[35] Ulaganathan S, Couckuyt I, Dhaene T, Laermans E, Degroote J. On the use of gradients in Kriging surrogate models. Proc Winter Simulation Conf. 2014, Savanah, GA, 2014:2692–2701. https://doi.org/10.1109/WSC.2014.7020113

[36] Queipo NV, Haftka RT, Shyy W, Goel T, Vaidynathan R, Tucker PK. Surrogate based analysis and optimization. Progr Aerosp Sci. 2005;41:1–28. https://doi.org/10.1016/j.paerosci.2005.02.001

[37] Dong J, Li Q, Deng L. Fast multi-objective optimization of multi-parameter antenna structures based on improved MOEA/D with surrogate-assisted model. AEU – Int J Electr Comm. 2017;72:192–199. https://doi.org/10.1016/j.aeue.2016.12.007

[38] Barmuta P, Ferranti F, Lukasik K, Gibiino GP. Schreurs D. Hybrid nonlinear model for microwave active devices using kriging. 2017 Integr Nonlinear Microwave Millimetre-wave Circuits Workshop (INMMiC), Graz, 2017:1–3. https://doi.org/10.1109/INMMIC.2017.7927317

[39] Morris MD, Mitchell TJ, Ylvisaker D. Bayesian design and analysis of computer experiments: use of derivatives in surface prediction. Technometrics. 1993;35:243–255. https://doi.org/10.1080/00401706.1993.10485320

[40] Journel AG, Huijbregts CJ. Mining geostatistics. London: Academic Press; 1981.

[41] Stein ML, Interpolation of spatial data: Some theory for kriging. New York: Springer; 1999.

[42] Rezaei A, Yahya SI, Jamaluddin MH. A novel microstrip diplexer with compact size and high isolation for GSM applications. AEU – Int J Electr Comm. 2020;114:153018. https://doi.org/10.1016/j.aeue.2019.153018

[43] Guan X, Yang F, Liu H, Zhu L. Compact and high-isolation diplexer using dual-mode stub-loaded resonators. IEEE Microwave Wireless Comp Lett. 2014;24:385–387. https://doi.org/10.1109/LMWC.2014.2313591